Detection of Lambda- and Omega-vortices with the temperature-tensitive paint method in the late stage of controlled laminar-turbulent transition*

Jonathan Lemarechal[¶,†], C. Klein[¶], U. Henne[¶], D. Puckert[°], U. Rist[°]

[¶] Deutsches Zentrum für Luft- und Raumfahrt e.V. (DLR),
Bunsenstraße 10, D-37073 Göttingen, Germany, jonathan.lemarechal@dlr.de
[°] Institut für Aerodynamik und Gasdynamik, Universität Stuttgart
Pfaffenwaldring 21, D-70569 Stuttgart, Germany

Abstract

An experiment investigating the laminar-turbulent transition of a Blasius boundary-layer like flow was set up in the laminar water channel at the Institute of Aerodynamics and Gas Dynamics, University of Stuttgart. The late stage of controlled transition with K-type breakdown was investigated with the Temperature-Sensitive Paint (TSP) method on the flat plate surface. Additional velocity measurements in the boundary layer were performed with the hot-film anemometry for better interpretation of the TSP results. The test conditions enable the TSP method to resolve the complete transition process temporally and spatially. Therefore, it was possible to detect the coherent structures occurring in the late stage of laminar-turbulent transition from the visualizations on the flat-plate surface: namely Λ- and Ω-vortices. The transition location is derived from the TSP visualizations with a gradient-based method and with the Turbulence Energy Recognition Algorithm (TERA) from the velocity measurements. The derived average transition location shows good agreement between the two techniques but the TSP method detected a later beginning and earlier end of transition.

Keywords *— Temperature-Sensitve Paint method, TSP, controlled transition, laminar-turbulent transition, K-type transition, Lambda-vortex, Omega-vortex*

1. Introduction

The laminar-turbulent transition of a two-dimensional wall-bounded shear layer in a low turbulence environment is divided into three phases before the boundary layer becomes fully turbulent (Kachanov, 1994): receptivity, linear stability, and nonlinear breakdown. The nonlinear development of transition was later refined by Guo et al. (2010), who divided this phase into weakly-nonlinear instability, late nonlinear stages, and super-late stages. In the late nonlinear stages the formation of vortical structures is observed. In order to investigate these phenomena it is beneficial to achieve a periodic flow with fixed flow structures.

One possibility to investigate laminar-turbulent transition with initially deterministic behavior and repeatability is provided by controlled transition with K-type breakdown. This type of transition, which is also named fundamental type, is characterized by spanwise alternating regions of high and low disturbance amplitude, which are called peaks and valleys, respectively. The experiment of Klebanoff et al. (1962) was the first to achieve this ordered peak-valley structure. In their experiment they used a vibrating ribbon, as implemented before by Schubauer and Skramstad (1948), and modulated the two-dimensional disturbance of the vibrating ribbon with so-called spacers. The modulation leads to a deformation of the disturbance and vortical structures which are called Λ-vortices develop in the nonlinear stages in the peak planes. The term Λ-vortex was derived from hydrogen-bubble visualizations performed by Hama and Nutant (1963). These vortices cause sweep and ejection events, which means that fluid is moved towards the wall and away from the wall, respectively. Guo et al. (2010) described that the sweep event of the Λ-vortex generates high-speed streaks near the wall. One possibility to investigate laminar-turbulent transition with initially deterministic behavior and repeatability is provided by controlled transition with K-type breakdown. This type of transition, which is also named fundamental type, is characterized by spanwise alternating regions of high and low disturbance amplitude, which are called peaks and valleys, respectively. The experiment of Klebanoff et al. (1962) was the first to achieve this ordered peak-valley struc-

*Citation and credit: Lemarechal, J., Klein, C., Henne, U., Puckert, D.P., Rist, U.: Detection of Lambda- and Omega-vortices with the temperature-sensitive paint method in the late stage of controlled laminar-turbulent transition. Exp Fluids (2019) 60:91 doi:10.1007/s00348-019-2734-1

†Corresponding author

ture. In their experiment they used a vibrating ribbon, as implemented before by Schubauer and Skramstad (1948), and modulated the two dimensional disturbance of the vibrating ribbon with so called spacers. The modulation leads to a deformation of the disturbance and vortical structures develop in the nonlinear stages in the peak planes, which are called Λ-vortices. The term Λ-vortex was derived from hydrogen-bubble visualizations performed by Hama and Nutant (1963). These vortices cause sweep and ejection events, which means that fluid is moved towards the wall and away from the wall, respectively. Guo et al. (2010) described that the sweep event of the Λ-vortex generates high-speed streaks near the wall.

The Λ-vortices stretch as they are convected downstream. In the late stages of transition, the stretched legs of the Λ-vortex reconnect at the downstream end and form an Ω-vortex, but both structures are initially still connected. Finally, the Ω-vortex detaches from the Λ-vortex and further evolves into a ring-like vortex by reconnecting its legs (Bake et al., 2002). This mechanism generates multiple ring-like vortices from a single Λ-vortex.

Velocity measurements in the peak region close to the transition encounter high-frequency velocity fluctuations of large amplitude, which are named spikes. These high-frequency velocity disturbances were found in experiments from Borodulin and Kachanov (1989) to occur in the center of ring-like vortices, which are formed at the tip of Λ-vortices as discussed. These experimental findings were later confirmed by DNS findings of Rist (1990) and Rist and Fasel (1995).

The ring-like vortices generated from a Λ-vortex are connected by a weak shear layer. This shear layer is weak because the strongly rotating legs of the Ω-vortex move quickly to the wall instead of moving fluid higher into the boundary layer. This shear layer close to the wall is subsequently stretched in streamwise direction. This phenomenon is described in detail by Borodulin et al. (2002) from experiments and DNS simulations and Bake et al. (2002) based on DNS simulations.

In addition Guo et al. (2010) described fluid quickly moving to the surface from experiments with hydrogen-bubble visualizations. They described the interaction of two sweep events, which occured during the interaction of a Ω-vortex with the Λ-vortex of the previous cycle. The sweep events of both structures combine and generate strong parallel high-speed streaks at the wall.

With the formation of the ring-like vortices, which cause the spikes, the randomization of the flow starts. The randomization of the ring-like vortices was described to begin as phase jitter or amplitude modulation by Borodulin et al. (2002) and Bake et al. (2002). This explains the minor variations of the location in which the structures appear. The repeatability is quickly reduced, which makes it more difficult to investigate it experimentally.

The structures occurring in the late stage of transition, i.e., Λ-vortices, Ω-vortices, and ring-like vortices, are summarized as coherent structures, see Kachanov (1994), Borodulin et al. (2002), and Bake et al. (2002). This makes the late stage of transition similar to fully turbulent flow, where hairpin vortices are coherent structures of similar size and shape, see Adrian (2007).

The Temperature-Sensitive Paint (TSP) method is a surface-based flow visualization technique that can be used for transition measurements in a variety of applications, e.g. cryogenic facilities (Fey et al., 2007), rotating systems (Weiss et al., 2017), and low-speed atmospheric wind tunnels (Lemarechal et al., 2018a). It has also been used for visualizations on a cylinder in crossflow in water facilities at different Reynolds numbers (Fey et al., 2013; Capone et al., 2015). In these experiments, the oscillation of the separation line and flow structures influencing the skin friction were visualized on the cylinder surface. The low flow speeds in water facilities and good heat transfer of water enable the TSP method to perform time-resolved flow visualizations with high spatial resolution over large areas with acceptable effort.

The TSP method visualizes differences in skin friction, which can be caused by laminar-turbulent transition or vortices. The increasing intermittency of the flow as part of the transition process increases the skin friction, which makes the TSP method an ideal technique to measure large areas of intermittent flow given that the temporal resolution of the flow is sufficient. Narasimha (1985) proposed measuring the intermittency on the surface as the intermittency is a surface quantity. It was shown by Owen (1970) that the intermittency measured inside the boundary layer below $y/\delta < 0.3$ agrees very well with values at the wall. Regions of high vorticity and strong random velocity fluctuations are generated close to the wall and grow in the downstream direction (Bake et al., 2002).

The laminar water channel has proven to be a viable facility to investigate Λ-vortices in previous experiments, see Kruse and Wagner (1998). Therefore, the TSP method with its possibility to measure large areas with high spatial resolution simultane-

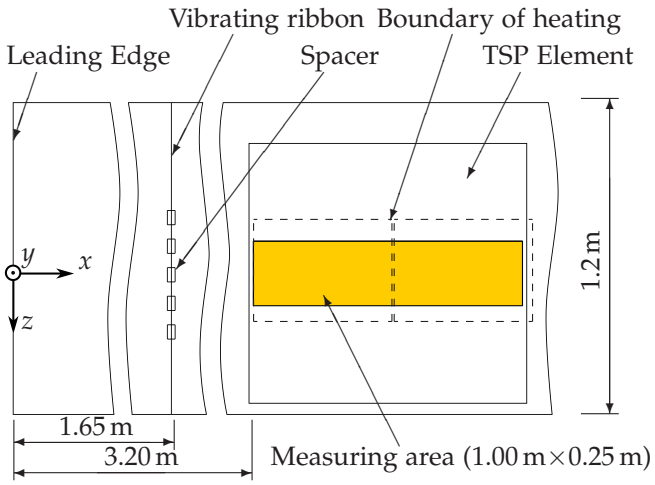

Figure 1: *Top view of experimental setup and definition of coordinate system.*

ously is used in this facility to investigate late stages of transition where the randomization process of the transition started (Borodulin et al., 2002; Bake et al., 2002). Investigations of laminar-turbulent transition on a flat plate in water has not been successfully performed with TSP prior to the present work, of which parts were shown in Lemarechal et al. (2018b). During the test in the laminar water channel with TSP additional hot-film measurements were performed for validating the TSP results. The present TSP measurements are the first time-resolved surface visualization with high spatial resolution of laminar-turbulent transition with sufficient temporal resolution to capture all relevant phenomena at the wall.

2. Experimental methods

To investigate the late stages of controlled laminar-turbulent transition the experiment was set up as shown in Fig. 1. The experiment consisted of two main parts, i.e., the disturbance excitation and a device to enable TSP measurements, which is called TSP element. The coordinate system used throughout this paper is also defined in Fig. 1. The current test was performed at a flow speed of $U_\infty = 0.12\,\mathrm{m/s}$ with the velocity variation being smaller than 1 %.

2.1. The laminar water channel

The experiments were conducted in the laminar water channel (âĂIJLaminarwasserkanalâĂİ) at the Institute of Aerodynamics and Gas Dynamics, University of Stuttgart. It was specifically designed for experiments investigating boundary-layer transition (Strunz and Speth, 1987) and provides a velocity range from 0.05 m/s to 0.2 m/s. The facility is characterized by a low turbulence level of $Tu = 0.05\,\%$ at 0.145 m/s in the relevant frequency range of 0.1 Hz to 10 Hz (Wiegand et al., 1995). A flat plate of 8 m length, 1.2 m width, and 8 mm thickness with an elliptic leading edge (10:1 axis ratio) is installed in the test section. On top of the flat plate the water level is 0.15 m high and has a free water surface. The facility provides easy optical access, which is very beneficial for the application of TSP. Along the flat plate the pressure gradient is close to zero and a Blasius boundary-layer like flow develops. To avoid contamination with turbulent flow the fluid of the unstable boundary layer in the corner of the flat plate and the side walls is sucked underneath the flat plate. The fluid is sucked through a slit between the flat plate and the side walls. A screen at the end of the flat plate generates the necessary pressure difference between the top and bottom of the flat plate (Kruse and Wagner, 1998). The facility is designed to minimize the temperature drift ($\Delta T < \pm 0.1\,\mathrm{K/day}$) even over longer time periods to enable long measurement times without significant Reynolds number drift.

2.2. Disturbance excitation

In order to achieve K-type transition a controlled two-dimensional disturbance needs to be introduced with sufficient amplitude. This disturbance needs to start growing soon after; therefore, the disturbance is introduced close to branch I of the stability diagram or further downstream (Kachanov and Levchenko, 1984).

At the laminar water channel, a vibrating ribbon is used to introduce two-dimensional Tollmien-Schlichting disturbances. With this device, the characteristics of the stability of the boundary layer were compared to theory. It was verified by Kruse (2016) that the boundary-layer stability of the laminar water channel is in good agreement with the Blasius boundary layer, which can be seen in Fig. 2. The agreement is best for lower dimensionless frequencies $F = 2\pi f U_\infty^{-2} \times 10^6 < 220$.

The vibrating ribbon consisted of a horizontally tightened wire with a diameter of 0.1 mm spanned across the entire test section width. The up and down motion of the wire was induced by an eccentric wheel mounted on a stepper motor, which drives a push rod on each side of the test section. The support for the vibrating ribbon is covered by a streamlined fairing. In combination with the reduced flow speed the sup-

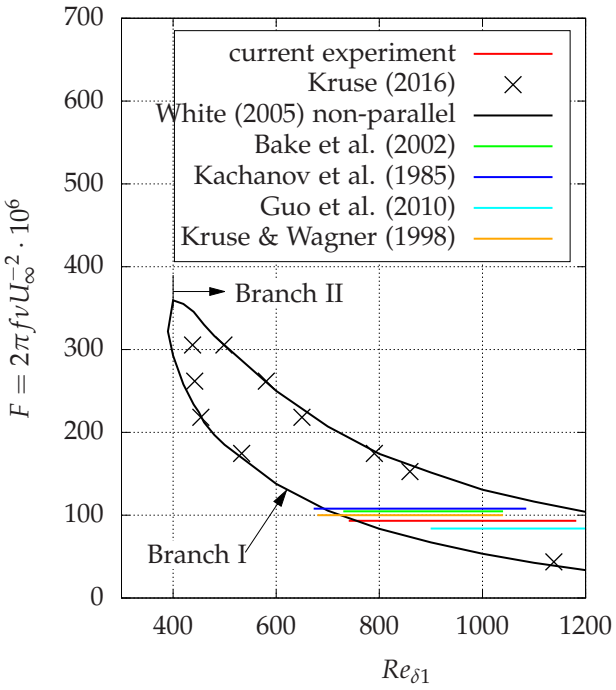

Figure 2: *Stability diagram, location of disturbance introduction and measuring area. Conditions are compared to published work of other authors.*

port does not cause turbulent wedges as observed by Kruse (1997). To get a reference signal for the TSP and hot-film measurements the position of the vibrating ribbon was measured with an inductive displacement sensor.

In the current experiment a lower disturbance frequency than in a previous experiment investigating Λ-vortices in this facility (Kruse and Wagner, 1998) was chosen: 0.2 Hz ($F = 90$). In order to introduce the disturbance close to branch I of the stability diagram, the vibrating ribbon is located further downstream at $x = 1.65$ m (Reynolds number based on the displacement thickness: $Re_{\delta 1} = 740$), see Fig. 2. The amplitude of the vibrating ribbon was chosen to be $y_A = 0.25$ mm, which generates Tollmien-Schlichting waves which evolve in agreement with linear stability theory. The wire has a zero position inside of the critical layer, i.e., in a height of $y = 6$ mm (Reynolds number based on wire diameter: $Re_d \approx 8$).

As in the experiments of Klebanoff et al. (1962), Kachanov (1985), and Kruse and Wagner (1998), additional spacers were needed to create the ordered Λ-vortex pattern characteristic for the K-type transition. The spacers ($x \times y \times z = 30\,\text{mm} \times 1\,\text{mm} \times 55\,\text{mm}$) are placed underneath the vibrating ribbon and were used to introduce a spanwise wavelength of $\lambda_z =$ 0.11 m. The height of the spacers of 1.0 mm was adopted from Kruse and Wagner (1998).

As can be seen in Fig. 2, the conditions of the disturbance and the flow conditions are comparable to experiments (Kachanov, 1985; Kruse and Wagner, 1998; Bake et al., 2002; Guo et al., 2010) and direct numerical calculations (DNS) (Rist and Fasel, 1995; Bake et al., 2002) in literature.

3. Measurement Techniques

The controlled transition is investigated with two measurement techniques: the Temperature-Sensitive Paint (TSP) method for surface visualization and hot-film anemometry to measure the streamwise (u) velocity component. The measurement techniques were not applied in parallel but the TSP method was used directly after the hot-film calibration and just before the hot-film measurements to check the flow conditions. Hence, the operation of the laminar water channel was not interrupted. Here, the TSP method proved very useful to recheck the flow conditions because of its short measurement and evaluation time. Afterwards, the time-consuming hot-film measurements were performed.

3.1. Temperature-Sensitive Paint method

The TSP method is a thermographic measurement technique to measure surface temperature distributions. The technique relies on the temperature-dependent emission of the fluorescence or phosphorescence light of certain dye molecules embedded in a surface coating. The molecules are excited by light of a suitable wavelength, e.g. from a light-emitting diode (LED), and the emitted light is recorded with a camera and stored as intensities I. Further details on the photophysics of TSP are given by Liu and Sullivan (2005).

The TSP method is a reversible flow visualization technique with a high density of stationary probes, i.e., TSP molecules or pixels, respectively. It can be considered non-intrusive because the surface coating can be integrated into the model surface and can also be polished. To perform flow visualizations with the TSP method, a heat flux between surface and fluid is necessary, see Fey and Egami (2007). For a constant heat flux, the local temperature difference between surface and fluid is depending directly on the local skin friction. This relation is called Reynolds analogy for Prandtl numbers close to unity, e.g. air, and Colburn analogy for Prandtl numbers unequal to one

(Lin, 1994), e.g. water. In the current work the skin friction is only qualitatively described because for unsteady flows the phase difference between thermal and velocity field are unknown, Rudolph (2011).

To enable TSP visualizations in the laminar water channel a movable device which provides a model heating and a substrate for the TSP coating was designed. A single current-carrying carbon fiber layer generates the necessary temperature difference between surface and fluid. This type of resistance heating was proposed by Fey and Egami (2007) and was applied in a low-speed wind tunnel test by Petzold and Radespiel (2015). In the following the layer design of the TSP element, which is shown in Fig. 3, is described from bottom to top. The foundation of the TSP element consists of an aluminum sheet of 1 mm thickness. Onto the aluminum sheet two layers of glass fiber with a combined thickness of $d \approx 0.36\,\text{mm}$ and the current-carry carbon fiber layer ($d \approx 0.26\,\text{mm}$) were laminated. The heating was split in two parts in streamwise direction for redundancy. Each heating part has a size of 500 mm by 300 mm and a resistance of 0.2 Ω between the contacts. Afterwards, a layer of glass fiber ($d \approx 0.18\,\text{mm}$), a layer of aluminum foil ($d \approx 0.05\,\text{mm}$) and two glass fiber layers (combined thickness: $d \approx 0.1\,\text{mm}$) were applied. The final layer of the TSP element is the TSP coating with a thickness of approximately 0.04 mm. The total thickness of the TSP element is approximately 1.9 mm. The leading edge of the the TSP element was designed to split the height of the TSP element into two forward-facing steps. The first forward-facing step is caused by the aluminum sheet metal with a height of 1 mm, see Fig. 3. This first step is followed after approximately 20 mm by the second forward-facing step, which is approximately 0.9 mm high, caused by the fiber reinforced plastic and the TSP coating. The thickness of the TSP element generates a two-step forward-facing step at the upstream end of the TSP element. Further details about the TSP element is given by Lemarechal et al. (2018c).

For the experiments in the laminar water channel, a TSP based on an Europium complex was applied. This TSP is characterized by high temperature sensitivity (3.3 %/K at 20 °C), negligible pressure sensitivity and a lifetime of approximately 300 µs, for more details see Ondrus et al. (2015).

Figure 4 shows the setup of the TSP measurement consisting of the TSP element, three scientific black-and-white cameras (PCO.4000), and four LEDs (HARDsoft IL-105/6X Illuminator UV). Optical bandpass filters were put in front of the cameras (center wavelength 630 nm, band width 75 nm) and LEDs (center wavelength 385 nm, band width 70 nm) to improve signal-to-noise ratio. In the presented experiment, the TSP method was used in the intensity method. The four LEDs have a peak emission at 405 nm and were set to a continuous output with a light power of approximately 3.5 W each. These settings were capable to excite the TSP molecules and gather sufficient luminescence light emission. The luminescence light of the entire coated surface ($x \times z = 1.00\,\text{m} \times 0.25\,\text{m}$) was recorded by the three cameras with 10 Hz acquisition rate and an exposure time of 4.5 ms. The chosen camera parameter result in 50 acquisitions per disturbance period and the exposure is short enough to result in subpixel displacement during the image acquisition. The optical setup produced an image resolution of 4.4 px/mm. This image resolution resulted in approximately 480 px per spanwise wavelength λ_z and approximately 88 px per 100 viscous units.

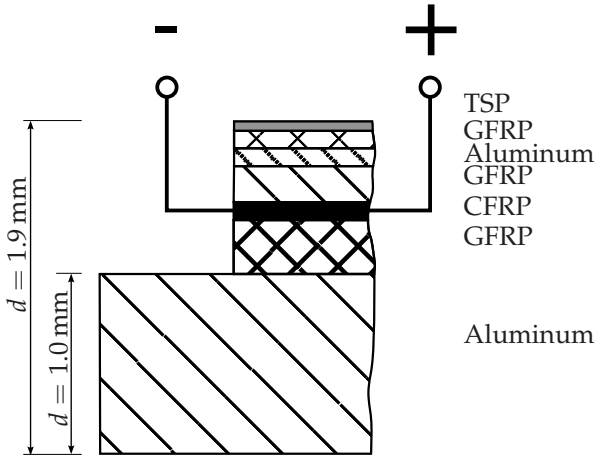

Figure 3: *Sectional view of the layers of the TSP element at the upstream end of the TSP element (not to scale). The abbreviations GFRP and CFRP denote the layers of glass fiber reinforced plastic and carbon fiber reinforced plastic, respectively*

In the following a brief description of the measuring sequence, which consisted of four phases, is given. Images were taken only in three of the four phases. In the first phase images were acquired without excitation light to quantify the background light. These are called dark images with the intensities I_{dark}. The next phase is characterized by the surface temperature and fluid temperature being in equilibrium and the TSP was excited. These images serve as reference images (I_{ref}) for the illumination pattern and the dis-

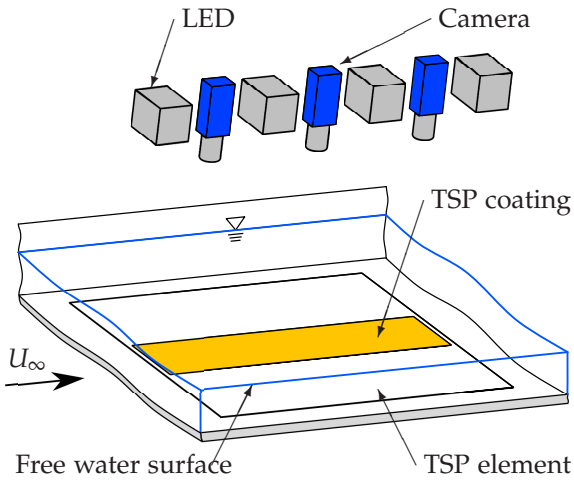

Figure 4: *Setup for TSP measurements in the laminar water channel.*

tribution of the TSP dye molecules. In the next phase, i.e., the heating phase, the heating was started with a constant electrical power of $P_{el} = 120\,\mathrm{W}$, which is a heating power of $400\,\mathrm{W/m^2}$. When a constant surface temperature was reached in the laminar regions the acquisition phase started. The chosen electrical heating power resulted in the surface temperature being $\Delta T \leq 1\,\mathrm{K}$ higher than the fluid temperature in laminar regions. In the acquisition phase, 900 images were acquired for each data point, which equals to 18 periods of the introduced disturbance. These intensities (I) were recorded at constant heat flux between surface and fluid. See Lemarechal et al. (2018c) for further details on the phases, conditions, and the timing.

The evaluation of the TSP images was performed partially using the in-house software nToPas, which was developed by Klein et al. (2005). In the first step of the evaluation the images of each phase were averaged to derive $\bar{I}_{dark}$, $\bar{I}_{ref}$, and $\bar{I}$. Subsequently the intensities $\bar{I}_{dark}$ of the averaged dark image is subtracted from averaged reference $\bar{I}_{ref}$, the averaged time series $\bar{I}$, and the time series I. Then the images are devided to derive the average result $\bar{I}_{ref}/\bar{I}$ and the time-series results $\bar{I}_{ref}/I$. An alignment of the images was not necessary because of negligible model movement and wave motion. Finally, the images are mapped onto a structured surface grid of 1 mm by 1 mm resolution. Further details on these initial steps of the TSP evaluation are given by Lemarechal et al. (2018c).

Afterwards, the time-series data were filtered with a single value decomposition (SVD) filter to reduce image noise (Pastuhoff et al., 2013). The data SVD filtering is a simplified procedure of the procedure presented in Lemarechal et al. (2018b): Only 75 modes are used for reconstruction, because it was realized that mode 76 and higher only contain camera noise. Afterwards, low-pass filtering (cut-off frequency of 1 Hz) is applied to each grid point to remove structures caused by the camera. Furthermore, the filtered data are used to calculate the standard deviation and amplitude spectrum via Fourier analysis of each grid point. Finally, the phase-averaged results are derived from the filtered time-series.

Two established methods to derive the location of laminar-turbulent transition from thermographic measurement techniques exist: a differential thermography used for both infrared technique (Raffel et al., 2015) and TSP method (Yorita et al., 2018) as well as a gradient based method (Ashill et al., 1996). The differential method is beneficial for oscillating profiles, where a significant movement of the laminar turbulent transition is to be expected. In the present experiment, however, the movement of the transition location is expected to be small; therefore, only the gradient-based method is applied. To derive the transition location from the TSP data the mean TSP image data were spatially median filtered ($x \times z = 20\,\mathrm{mm} \times 5\,\mathrm{mm}$). Afterwards, a polynomial was fitted to the derivative $\partial(\bar{I}_{ref}/\bar{I})/\partial x$ of the intensity ratio distribution in x-direction. The transition location was set to be at the minimum of the polynomial.

3.2. Hot-film anemometry

A single-wire hot-film probe (Dantec 55R15) was used in constant temperature (CTA) mode with a wire-to-fluid-temperature ratio of 1.08. The probe was used to measure the $u = \bar{u} + u'$ velocity component in main flow direction. The hot-film probe was calibrated before the measurement using the traversing system of the laminar water channel and the method described by Subasi et al. (2015).

The hot-film measurement was performed parallel to the surface of the TSP element at a constant height of $y = 7\,\mathrm{mm}$. This places the hot-film probe in the critical layer of the boundary layer in which the disturbances are much larger than the signature of the disturbances at the wall.

The measuring area ranged from $3.2\,\mathrm{m} \leq x \leq 4.25\,\mathrm{m}$ and $-0.12\,\mathrm{m} \leq z \leq 0.12\,\mathrm{m}$ in steps of $\Delta x = 25\,\mathrm{mm}$ and $\Delta z = 10\,\mathrm{mm}$. A data point was acquired over 30 s with 100 Hz acquisition frequency. These settings result in resolving the spanwise wavelength

with 4 data points and an acquisition of 6 phases per data point.

With the hot-film measurement above the TSP element the disturbances of the forward-facing step of the TSP element are included in the measurement of the u velocity component. The model heating is only used during the TSP measurements. Because of that, the hot-film results are not influenced by the heating. Therefore, the hot-film measurements can be used to determine the influence of the model heating on the transition location.

4. Results and discussions

In the first step of the evaluation the K-typ transition is investigated with the help of averaged and statistically evaluated results of both measurement techniques. In the second step the unsteady flow field is examined with phase-averaged results of both measurement techniques and TSP time-series results. All results are presented in top view, i.e., the xz-plane.

4.1. Mean-flow results

Initially, the hot-film measurements are presented as the maximum velocity fluctuation u'_{max} in Fig. 5. They clearly show the developed peak and valley structure as described by Klebanoff et al. (1962). The peaks and valleys can be clearly identified in Fig. 5 as regions of high and low maximum velocity fluctuation, respectively. The spanwise distance between the centers of two peak structures equals the introduced spanwise wavelength λ_z and the width of a peak equals half this wavelength. In the center of each peak an area of significantly higher maximum velocity is visible from approximately 3.5 m to 3.7 m. This region is caused by high-frequency velocity fluctuations, called spikes. The velocity measurements presented here were performed inside of the boundary layer, this is not where the center of these structures passes. Despite their center being located higher in the boundary layer, these coherent structures can be detected because of their strong shear layer that reaches lower into the boundary layer (Borodulin et al., 2002; Bake et al., 2002). The shear layer caused the spikes in the hot-film measurement. The peak on the negative z-side is wider than on the positive z-side, which is expected to be a side structure of the Λ-vortices (Fig. 5). This asymmetry is very likely caused by the spacers. Bake et al. (2002) reported that the evolution of Λ-vortices is very sensitive to the spacers' shape, distance, and orientation.

The results of the TSP measurements are shown in the form of mean result $\bar{I}_{ref}/\bar{I}$, standard deviation σ, and amplitude spectrum of a single frequency $|Y|$ in Fig. 6 a) to c). All results show the same peak and valley structure as the hot-film results but the side structure (Fig. 5) is only visible in the mean results as a blurred edge of the peak on the negative z-side (Fig. 6 a)). The TSP mean result visualizes areas of large and low skin friction as small (dark) and large (bright) intensity ratios ($\bar{I}_{ref}/\bar{I}$), respectively. Downstream of $x = 3.7$ m and 3.65 m very large skin friction (see Fig. 6 a)) is observed, which is assumed to be caused by mostly intermittent or fully turbulent flow. This assumption is confirmed by the distribution of the intermittency factor $\gamma = 0.5$ in Fig. 7 as evaluated from hot-film velocity measurements, which are discussed later. These regions of high intermittency is wedge shaped and the wedges are united from $x = 4.15$ m on.

The TSP average shows three parallel lines of increased skin friction in each peak that lead to the beginning of the high intermittency flow (indicated in Fig. 6 a)). These lines converge in the area where the velocity measurement detected the spikes. Between the peaks, the visualization and the velocity fluctuation indicate a high speed streak, i.e., a region of high velocity close to the wall that also leads to increased skin friction. The peak on the positive z-side is more sharp-edged than the one on the negative side, where the side of the peak closer to the center of the image is blurred (indicated in Fig. 6 a)). The same area has more intense velocity fluctuations u'_{max} than the other visible edges of the peaks, which can be seen in Fig. 5. The asymmetry starts already at $x = 3.4$ m as an area which shows a little increased skin friction compared the sides of the sharp-edged peak.

The standard deviation σ of the TSP data (Fig. 6 b)) highlights an area of large fluctuations in the tip of the area of high intermittency. At the same location, spikes were detected in the maximum velocity fluctuation u'_{max} in Fig. 5. Also the edges of the high intermittency area are visible. On the contrary, in the more turbulent region the values of the standard deviation σ decline again significantly, which could not be observed in the standard deviation of the velocity data (these are presented in Fig. 8b in Lemarechal et al. (2018b)). But it can be seen that the parallel structures leading to the tip of the wedge shaped high intermittency area are not steady. It is concluded that the local skin friction must be varied by the Λ-vortices. One vertical line in the middle of the average TSP result in 6 a) marks a gap in the heat

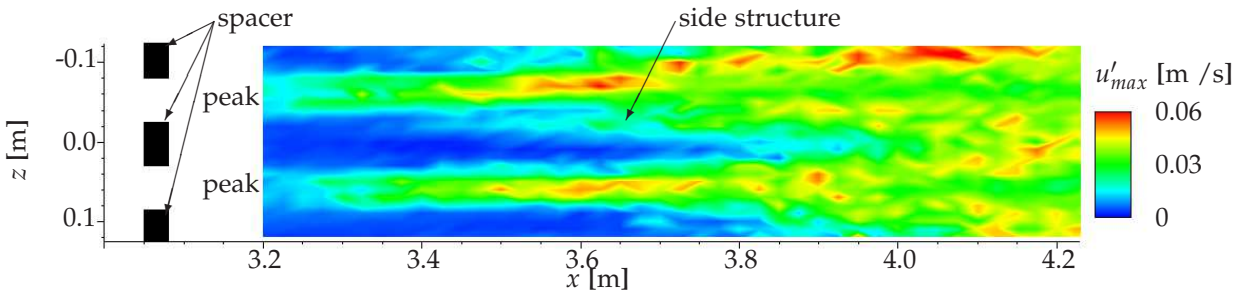

Figure 5: *Maximum velocity fluctuation u'_{max} in flow direction. The spanwise location of the spacers is displayed and the spanwise peak location between the spacers is depicted.*

flux, which is caused by the aforementioned gap between the two heating areas. The standard deviation in Fig. 6 b) does not show this gap, therefore, it is concluded that the measurement was started when the surface had reached a constant temperature.

To further investigate the structures in each peak at the beginning of the high intermittency area, the amplitude spectrum for the excitation frequency is derived via Fourier analysis. The result in Fig. 6 c) clearly shows that the fluctations of large amplitude oscillate with the disturbance frequency. However, the parallel lines leading to the beginning of the intermittency, which showed fluctuations in the standard deviation, hardly contain the disturbance frequency. Furthermore, it is visible that the area of high intermittency and turbulent flow coincide with regions of significant amplitude in the excitation frequency. This Fourier analysis registers the differences between laminar and intermittent flow better than the standard deviation, which emphasizes the region of transition where the largest gradients in the TSP results occur.

To compare the transition measurements quantitatively the transition location x_t is derived from both measurement techniques. The TSP time-series data which are presented in section 4.3 show no sign of turbulent spots, which can be observed with the TSP method (Lemarechal et al., 2018c). Therefore, the intermittency does not increase by more frequently occuring turbulent spots as described by Narasimha (1985). But the convective nature of the investigated instability causes the transition to move forth and back and thus the growing disturbances will cause an increasing intermittency factor γ. Due to this temporal variation of the laminar to turbulent ratio it was decided to calculate the intermittency for each streamwise hot-film measurement location to compare transition locations.

The intermittency was determined with the Turbulence Energy Recognition Algorithm (TERA) as presented by Falco and Gendrich (1990). The TERA method has proven to be a reliable method to detect laminar-turbulent transition in the laminar water channel, see Puckert and Rist (2018). The detector function $\mid u' \cdot \partial u'/\partial t \mid$ is calculated from appropriately filtered velocity data and afterwards the temporal fraction of laminar to turbulent flow is derived for each hot-film measurement location. An intermittency of $\gamma = 0$ and $\gamma = 1$ correspond to laminar and turbulent flow, respectively. From the intermittency data the transition location is determined where laminar and turbulent flow have the same temporal fraction, which corresponds to $\gamma = 0.5$. The transition location as determined by the hot-film anemometry is shown in Fig. 7. In line with Kachanov (1994), a rather quick evolution from laminar to turbulent flow, i.e., from $\gamma = 0$ to 1, can be seen. The intermittency increases later but more rapidly in the valley region, see Fig. 8 c).

The transition location as derived from the minimum of the spatial intensity gradient in x-direction enables also transition detection in the gap of the heat flux. The valleys prove difficulties to detect the transition location from the TSP mean result. This is caused by streaks, which reduce the intensity-ratio gradient at the transition location. Furthermore, the fully turbulent region is outside of the measurement area.

The transition location determined from the hot-film and TSP data are in good agreement, as can be seen in Fig. 7. The area of high fluctuations on the negative z-side is less pronounced in the transition location of the TSP visualization than in the hot-film measurement. Because the hot-film measurements were performed in 7 mm distance to the wall, which corresponds to $y/\delta \approx 0.3$. The result of Owen (1970) allows to conclude that the TSP technique with the gradient-based evaluation method measures the same transition location as the intermittency derived

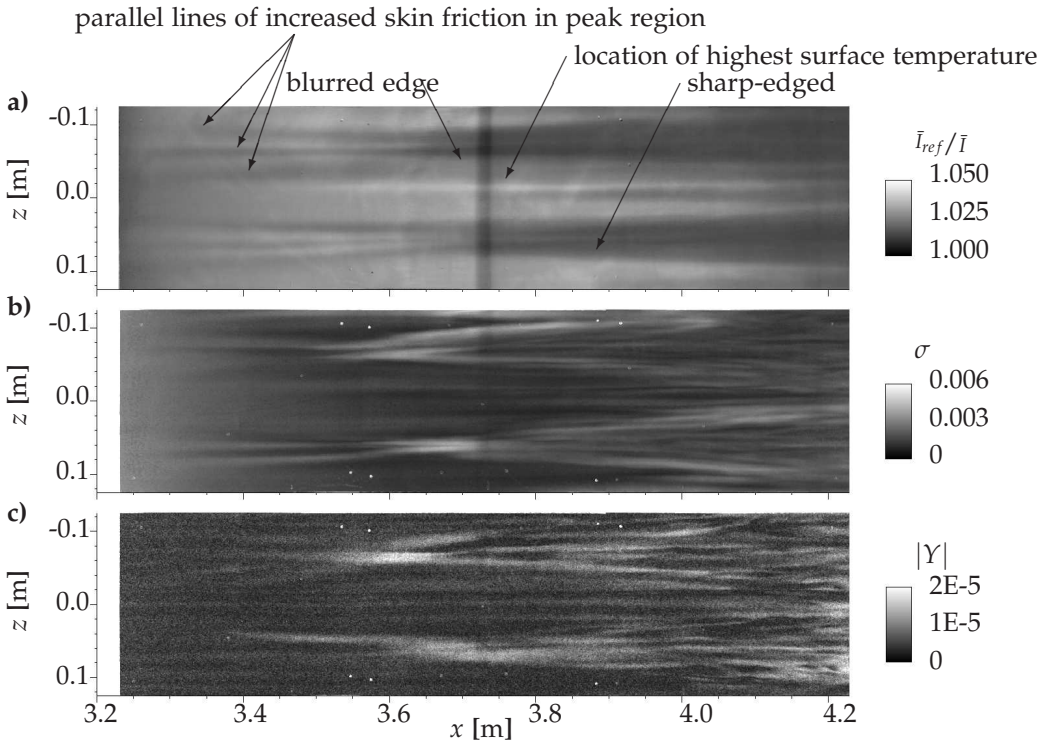

Figure 6: *Statistical influence of late stage of controlled transition on skin friction. a) mean result, b) standard deviation, and c) amplitude distribution for the excitation frequency, which was determined by means of Fourier analysis.*

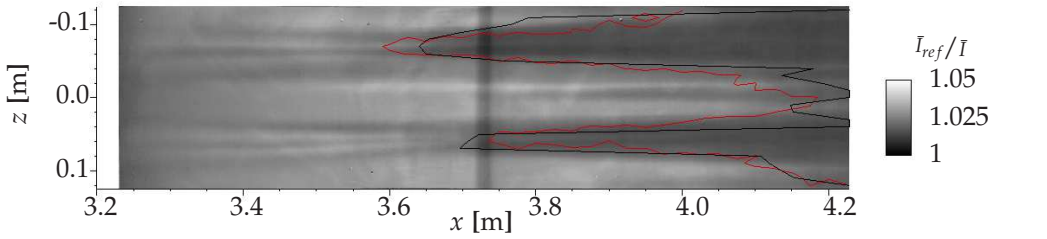

Figure 7: *The mean result of the TSP visualization is shown with the determined transition location from the TSP method (black) and from velocity measurement (red), which corresponds to* $\gamma = 0.5$.

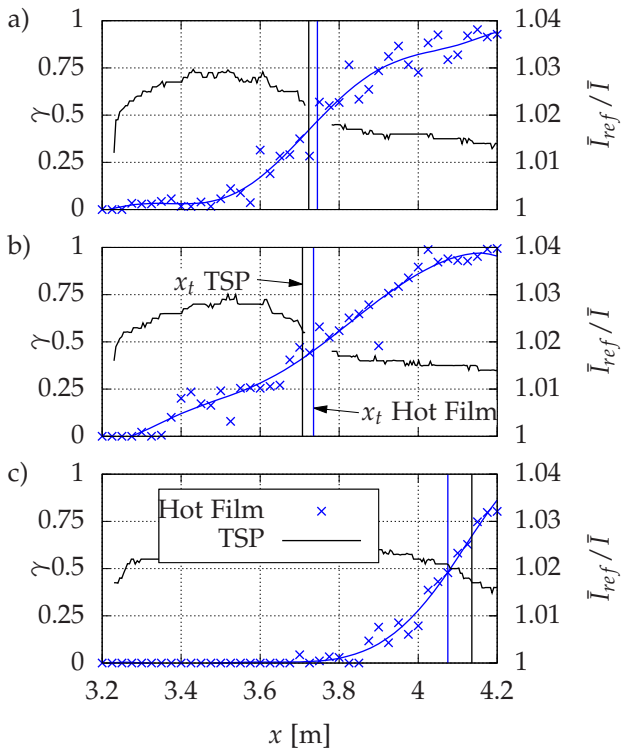

Figure 8: *Detailed comparison of transition locations on the basis of three streamwise slices at $z = 0.05\,\mathrm{m}$ a), $z = 0.06\,\mathrm{m}$ b), and $z = -0.03\,\mathrm{m}$ c). For better comparison the axis of the intensity ratio $\bar{I}_{ref}/\bar{I}$ is inverted to be directly a function of skin friction and therefore comparable to the intermittency. A 7^{th} order polynomial fit is used to show the development of the intermittency.*

from hot-film data. This is investigated in Fig. 8 for two locations in the vicinity of the peak ($z = 0.05\,\mathrm{m}$ and $z = 0.06\,\mathrm{m}$) and one in the valley ($z = -0.03\,\mathrm{m}$).

The intermittency data measured with the hot-film anemometry show the evolution from laminar to turbulent flow is well resolved and ranges over a large streamwise extent. In the peak region, the laminar-turbulent transition evolves over 0.6 m and $\gamma = 1$ is reached at the end of the measurement domain, see Fig. 8 a) and b). In contrast the flow in the valley region ($z = -0.03\,\mathrm{m}$ in Fig. 8 c)) does not reach the turbulent state, where the intermittency would reach $\gamma = 1$. On the other hand, the development of the TSP results is more complicated to interpret. At all three slices the intensity ratio $\bar{I}_{ref}/\bar{I}$ declines at first, which is caused by the beginning of a non-adiabatic surface at the leading edge of the TSP element. From $x = 3.4\,\mathrm{m}$ on a constant value of $\bar{I}_{ref}/\bar{I} \approx 1.03$ is reached in the peak region. This intensity ratio corresponds to laminar flow. The slice in Fig. 8 c) reaches at first a constant level of lower intensity ratio, i.e., larger skin friction, because the slice passes through the structures leading to the high intermittency area. But especially for the slices in the peak region (Fig. 8 a) and b)) the intermittency reached already $\gamma \approx 0.25$ before the TSP intensity ratio value decreases. Also the constant intensity ratio in the turbulent region $I_{ref}/I \approx 1.015$ is reached already when the intermittency reached only $\gamma \approx 0.6$.

From these results we have to conclude that the resolution of the transition zone is limited for the TSP method: The beginning and the end of transition is missed. Owen (1970) already observed that the change of the average velocity profile is small for $\gamma = 0.16$, which prevents measurement techniques relying on skin-friction or heat transfer changes to detect the same beginning of transition as techniques based on velocity fluctuation measurements.

4.2. Phase-averaged results

In the following the possibility to investigate the coherent structures of late stage of transition, i.e., Λ- and Ω-vortices, with TSP is demonstrated. For the presented K-type transition setup the occurrence of Λ-vortices is expected in the peak regions as previous experiments (Klebanoff et al., 1962; Hama and Nutant, 1963) and DNS simulations (Rist, 1990; Rist and Fasel, 1995). To detect the Λ-vortices from the single-probe hot-film measurements and to directly compare both measurement techniques the fluctuating quantity of both measurement techniques is phase averaged. To enable direct comparison, the hot-film data are laid over the TSP data. The phase-averaged data are presented in Fig. 9 for five different phases of the cycle $t/T = 0.2$, 0.4, 0.6, 0.8, and 1.0.

In the peak region, the phase-averaged velocity fluctuations u' are in the order of per mill and show alternating fluctuations greater and smaller than zero. These velocity fluctuations are Λ-shaped structures upstream of $x = 3.7\,\mathrm{m}$, which convect within the period in flow direction, see Fig. 9 a) to e). Falco and Gendrich (1990) assigned those to sweep and ejection events, respectively. In front of the Λ-vortex the sweep event moves high-speed fluid closer to the wall and behind the vortex the ejection events move low-speed fluid away from the wall. Therefore, the location of Λ-vortex is between a sweep and an ejection event. As expected, no phase-dependent fluctuations are visible in the valley region.

In the region where the Λ-shaped structures are observed in the velocity data also Λ-shaped periodic

skin-friction fluctuation are visible in the TSP data $\bar{I}_{ref}/\widetilde{(I-\bar{I})}$, see Fig. 9. The spanwise extent of both techniques is comparable and in the order of the width of the peak region. As can be seen in Fig. 9 a) to e) the Λ-shaped structures measured with each measurement technique have a constant phase relationship. Because the sweep of the Λ-vortex generates a high-speed streak at the wall (Guo et al., 2010), the skin friction is locally higher and can be detected by TSP. The TSP technique visualizes changes in skin friction; therefore, it is expected, that Λ-shaped structures are caused by the Λ-vortices. The vortex core is most likely above the location of largest skin friction, see Fig. 9, and the regions of smaller than average skin friction are expected to lie between two successive vortices.

After $x \approx 3.5\,\mathrm{m}$, the Λ-vortices elongate in streamwise direction significantly, which is visible in the velocity and skin-friction fluctuations, see Fig. 9 a) for example, where the Λ-vortex from the previous period, i.e., the Λ-vortex further downstream is narrower and longer. In DNS results Borodulin et al. (2002) and Bake et al. (2002) showed that at the location of the Λ-vortex stretching Ω-vortices and ring-like vortices are formed. At some point the Λ-vortex starts to interact with the upstream Λ-vortex of the previous cycle. This causes the shear layer belonging to the ring-like vortices to rapidly descent to the wall as described by Bake et al. (2002) from DNS results. Because the ring-like vortices cause the spikes u'_{max} (Fig. 5) has its maximum at the location where the phase averaged velocity fluctuations show the elongation of the Λ-vortices ($x = 3.5\,\mathrm{m}$ to $3.7\,\mathrm{m}$ in Fig. 9). Guo et al. (2010) found in hydrogen bubble visualizations that this interaction causes very strong sweep events because the sweep of the Ω-vortices' legs combine with the sweep of the following Λ-vortex and generate strong high-speed streaks at the wall. Because of that the skin-friction fluctuation develops its maximum at the rear end of the Λ-vortex underneath the area of negative u'. These strong fluctuations of the skin friction are caused by new structures impinging onto the surface. Two parallel streamwise oriented structures in the skin friction are expected. This is only visible on the positive z-side, see Fig. 9 d) and e). That is why this location is investigated in more detail in section 4.3.

Downstream of the location of maximum and minimum skin friction, i.e. at $x \approx 3.7\,\mathrm{m}$, the ordered structures become chaotic and their shape quickly changes. Approximately at this location both measurement techniques indicated the transition location in the peaks at $x = 3.6\,\mathrm{m}$ and $3.75\,\mathrm{m}$, respectively.

Only for few very large structures a relationship between the structures visible in the velocity and skin-friction fluctuation remains, e.g. at $x = 4.1\,\mathrm{m}$ and $z = 0.04\,\mathrm{m}$ in Fig. 9 d). The randomization process as described by Borodulin et al. (2002) and Bake et al. (2002) starts at $x \approx 3.7\,\mathrm{m}$, which is visible in the decreasing size of the structures in the phase average in Fig. 9.

The peak on the negative z-side showed an asymmetry on the side closer to the middle of the field of view in the form of a blurred edge of the peak in the average TSP result in Fig. 6 a). At the same location also the velocity fluctuations are increased, see Fig. 5. In the phase average results it is visible that at $x = 3.4\,\mathrm{m}$ a secondary structure develops on this side of the Λ-vortices of this peak structure. This secondary structure develops only on one side of the peak and forms an asymmetry. The secondary structure has a fix relation to the adjacent Λ-vortices. This structure seems to have insufficient influence on the skin friction in phase with the introduced disturbance to be captured in the phase-averaged TSP results, see Fig. 9, where no indication of this structure is visible. However, these asymmetric side structures are visible in the TSP average in Fig. 6 a) as a blurred edge of the peak. An example of symmetric structures occuring next to the Λ-vortices is visible in the DNS works from Bake et al. (2002).

4.3. Time-series results

The breakup of the Λ-vortices is further investigated with the TSP time-series results, because the expected parallel structures were not visible in both peak locations. For two phases ($t/T = 0.2, 0.4$) and three consecutive periods the instantaneous TSP result are shown in Fig. 10 a) to f). Only the area of the breakup of the Λ-vortices is shown and the range of the intensity ratio is compressed. The results of the Fourier analysis (Fig. 6 c)) and the phase-averaged results (Fig. 9) showed that this area is dominated by skin-friction fluctuations, which oscillate with the excitation frequency. In the time-series results two parallel, elongated areas of increased skin friction underneath the elongated Λ-vortex can be clearly identified. At the same location the elongated Λ-vortex can be observed in the velocity fluctuations u' in Fig. 10. Also the maximum of the velocity fluctuation was located there (Fig. 5), which led to the conclusion that Ω-vortices are formed in this area and impinge on the wall. These form two parallel high-speed streaks,

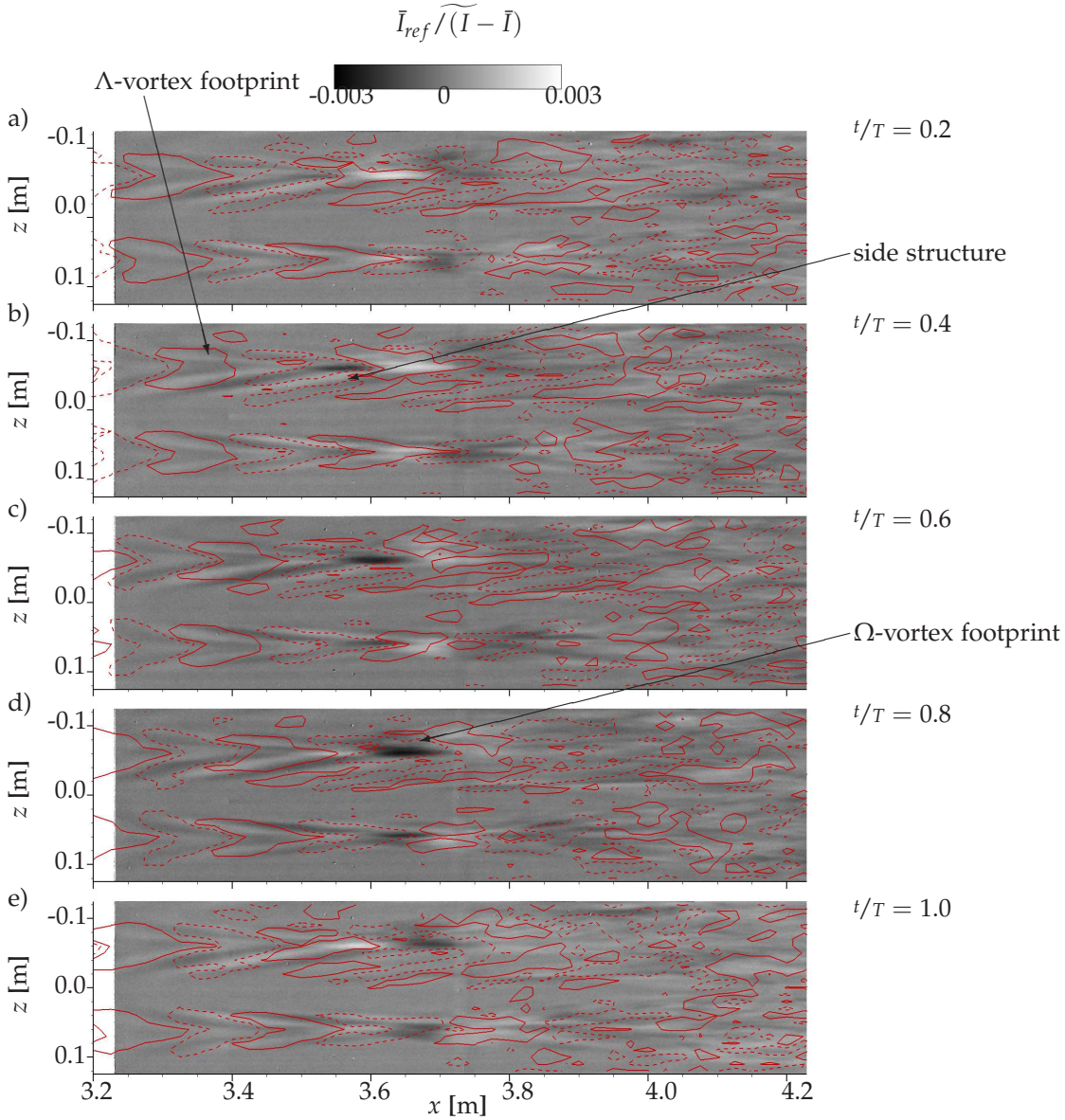

Figure 9: *Phase-averaged TSP and hot-film anemometry results for $t/T = 0.2$ a), 0.4 b), 0.6 c), 0.8 d), 1.0 e). Solid lines (–) equal $u' = 0.005\,\mathrm{m/s}$ and dashed lines (- - -) equal $u' = -0.005\,\mathrm{m/s}$.*

which are visible as parallel lines of increased skin friction, i.e., very low intensity ratio, in Fig. 10.

The three instances of time shown in Fig. 10 a) to c) show the same structure in the skin friction distribution but minor variances of the high-speed streaks, i.e. longitudinal streamwise structures of increased skin friction, are visible. They are separated by a low-speed streak, which is caused by fluid being lifted away from the wall by the vorticity of the legs of the ring-like vortex. This low-speed streak between the legs of a coherent structure was also described by Adrian (2007) for hairpin-vortices in a turbulent boundary layer. The streamwise start, the spanwise location and the strength varies for each period, which is a clear indication for the beginning randomization. But the trend of the legs to shift in negative z-direction when evolving in downstream direction is true for all periods.

Figure 10 d) to f) show later instances of the same period compared to Fig. 10 a) to c), respectively. The growth and elongation of the streaks is visible. This was already described by Bake et al. (2002) for the shear layer of the structures in the vicinity of the wall.

The findings from the phase averaged and time-series results are depicted in Fig. 11. The schematic shows the vortex cores of two Λ-vortices and one Ω-vortex above the TSP visualization for one peak region. Furthermore the vortices' cores are projected onto the TSP visualization to easier localize their position in relation to the TSP visualization. The other part of the visualization shows the footprint of the same vortex system.

4.4. Errors

By applying the TSP method in the laminar water channel, three possible disturbances are caused: two for-ward-facing steps of low height at the leading edge of the TSP element, thermally induced turbulence, and buoyance forces induced by the warmer surface of the TSP element.

The size of the forward-facing steps at the TSP element's leading edge is compared to the boundary layer to asses their influence on the flow. The ratio of the total height d of the two forward-facing steps to the local displacement thickness is approximately $d/\delta_1 \approx 0.21$. The experiments from Wang and Gaster (2005) on forward-facing steps in a boundary layer without pressure gradient predict that the transition location in the current setup will not be altered significantly by the step at the leading edge of the TSP element. The step will be avoided in future experiments by partially replacing the flat plate of the laminar water channel with an insert for TSP measurements.

Introducing thermal energy into the laminar water channel had to be limited in order to reduce the risk of generating thermally induced turbulence, which was already addressed during the design of the facility by Strunz and Speth (1987). Therefore, the spanwise extent of the model heating and the surface coated with TSP was limited to $\Delta z = 0.30\,\mathrm{m}$ and $\Delta z = 0.25\,\mathrm{m}$, respectively. The model heating is wider than the TSP coating because of reduced quality of the TSP results due to possible temperature inhomogeneity. Considering the spanwise wavelength introduced by the spacers just over two wavelengths can be resolved.

In the present experiment, the maximum temperature difference between fluid and surface is reached in the laminar flow in the valley region just before transition (the location of largest $\bar{I}_{ref}/\bar{I}$ in Fig. 6 a)) and is smaller than 1 K. To quantify the influence of the buoyancy forces caused by the non-adiabatic wall the Richardson number is used, see also Sabatino and Smith (2008) and Capone et al. (2015). The Richardson number Ri is equal to the Grashof number Gr_x divided by Reynolds number Re_x^2 squared and therefore defined as:

$$\mathrm{Ri} = \frac{\mathrm{Gr}_x}{\mathrm{Re}_x^2} = \frac{g\beta\,(T_w - T_\infty)\,x}{U_\infty^2}. \tag{1}$$

The temperature difference between the surface T_w and the fluid T_∞, the center of the measuring location x and the free stream velocity U_∞ are the variables during the measurement, which define the Richardson number. A balance between signal-to-noise ratio and bouyance forces has to be found.

For the conditions of the present experiment the Richardson number $Ri < 0.5$ predicts that the bouyancy forces cannot be neglected entirely, which is possible for $Ri \ll 0.1$ (Ghiaasiaan, 2011). But the surface is only heated in the late stages of transition, where the disturbances in the flow have already reached large amplitudes and deformed the two-dimensional flow into three-dimensional flow with peak-valley structure. Therefore, it is expected that buoyancy forces of significant strength cannot develop in the tested setup. Furthermore, the comparison of the hot-film results, which were performed with an adiabatic surface, and TSP results show excellent agreement. It is concluded that no new instabilities or additional destabilization of the boundary layer were introduced by the heating, which is necessary for non-intrusive thermographic measurements

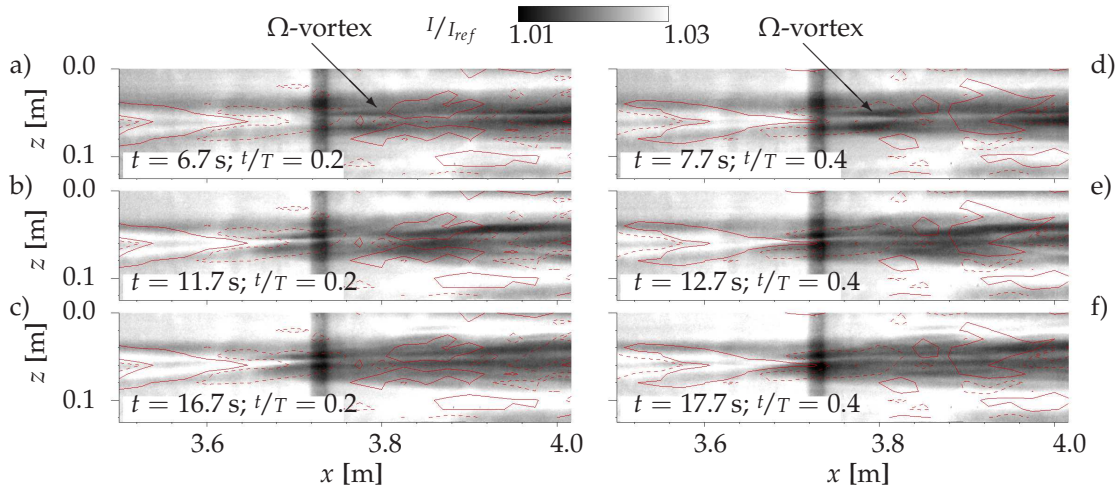

Figure 10: *Detail of instantaneous TSP result of the same phase as the same phase average result for the velocity fluctuations. For two different periods periods $t/T = 0.2$ and 0.4 and three consecutive cycles. Solid lines (–) equal $u' = 0.005\,\mathrm{m/s}$ and dashed lines (- - -) equal $u' = -0.005\,\mathrm{m/s}$.*

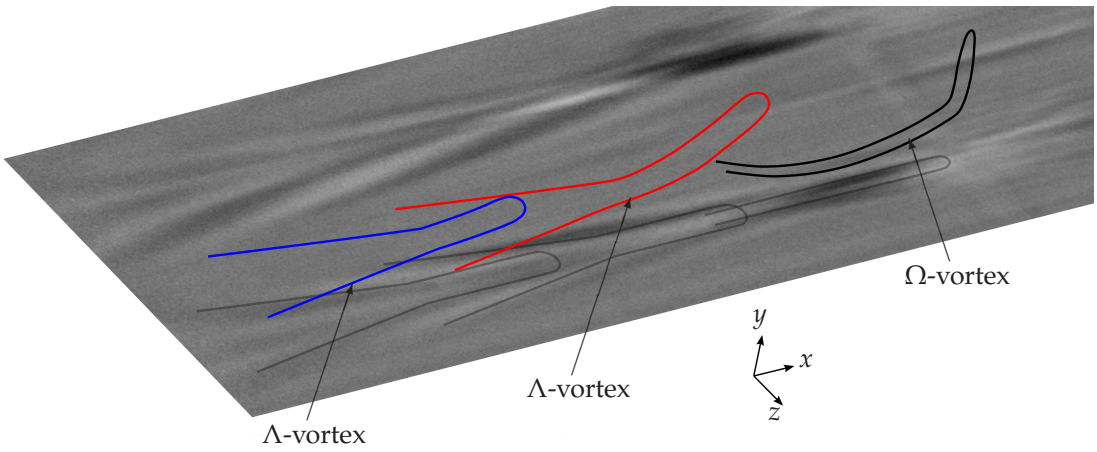

Figure 11: *A phase averaged TSP surface visualization of the late stage of K-type transition and a schematic of the vortex system. The flow direction is in x-direction and the cores of the voritices are sketched.*

in low-speed applications.

5. Conclusions

An experiment investigating controlled transition (K-type transition) was set up in the laminar water channel at the Institute of Aerodynamics and Gas Dynamics, University of Stuttgart. In the experiment the TSP method was successfully used to perform time-resolved surface visualizations in late-stage of the laminar-turbulent boundary-layer transition. To perform measurements with the TSP method, the measurement technique was adapted to the conditions of the laminar water channel, i.e. heating power and acquisition scheme. Furthermore, a device providing a substrate and the necessary model heating, which can be placed flexibly in the facility, was designed. The TSP visualizations were accompanied by velocity measurements in the boundary layer with hot-film anemometry. Both techniques are directly compared to improve the understanding of the TSP results. This combined measurement is new and the following results were derived:

- The mean transition location was determined from both measurement techniques. The results show that the transition location determined from the average TSP result is equal to 50 % intermittency. But the beginning of transition is detected further downstream and the end of transition further upstream by the TSP technique. The detected transition beginning is delayed in the TSP result because the change of the mean velocity profile for small intermittency values causes only small skin friction change (Owen, 1970).
- In the peak region Λ-vortices develop and cause sweep events, which change the skin friction. The TSP method is able to visualize Λ-shaped skin friction fluctuations after phase avering the acquired time series. The Λ-vortices could not be visualized in the time series because of an insufficient impact on skin friction.
- In the late stage of transition Λ-vortices generate Ω-vortices, the parallel legs of which impinge on the wall and elongate in streamwise direction (Borodulin et al., 2002; Bake et al., 2002). In the TSP time series the peak region shows parallel, elongated structures just before small-scale random structures occur. A constant phase relation between the visualized Λ-shaped structures and the elongated parallel structures is observed in the phase averaged results. Therefore, it is concluded that the TSP method visualizes the legs of the Ω-vortices. The stronger influence of the Ω-vortices on the skin friction is caused by strong sweeps as observed by Guo et al. (2010).

From the present experiments it can be concluded, that the TSP method is suitable for the investigation of coherent structures with a footprint on the wall, like Λ- or Ω-vortices. The major advantage of the technique is to perform a time-resolved measurement of a large area synchronously. This enables measurements also after the beginning of the randomization of the flow, i.e., turbulent flow, where phasen averaging is not feasable.

Acknowledgements The authors would like to thank Mr. Carsten Fuchs (DLR-AS-EXV), Mr. Tobias Kleindienst (DLR-AS-EXV), Dr. Vladimir Ondrus (University of Hohenheim), Ms. Esther Mäteling (RWTH Aachen University), and Mr. Martin Weberschock (Weberschock Development) for their support during the design, manufacturing, and preparation of the TSP element. We thank Mr. Daniel Kruse (University of Stuttgart) for measuring the boundary layer stability behaviour of the laminar water channel.

References

R.J. Adrian. Hairpin vortex organization in wall turbulence. *Physics of Fluids*, 19(041301), 2007.

P. Ashill, C. Betts, and I. Gaudet. A wind tunnel study of transition flows on a swept panel wing at high subsonic speeds. In *CEAS 2nd European Forum on Laminar Flow Technology*, pages 10.1–10.17, 1996.

S. Bake, D.G.W. Meyer, and U. Rist. Turbulence mechanism in Klebanoff transition: a quantitative comparison of experiment and direct numerical simulation. *J Fluid Mech*, 459:217–243, 2002.

V.I. Borodulin and Y.S. Kachanov. The role of the mechanism of the local secondary instability in k-breakdown of boundary layer. *Sov. J. Appl. Phys*, 3(2):70–81, 1989.

V.I. Borodulin, V.R. Gaponenko, Y.S. Kachanov, D.G.W. Meyer, U. Rist, Q.X. Lian, and C.B. Lee. Late-stage transitional boundary-layer strucutes. direct numerical simulation and experiment. *Theoret. Comput. Fluid Dynamics*, 15:317–337, 2002.

A. Capone, C. Klein, F. Di Felice, U. Beifuß, and M. Miozzi. Fast-response underwater TSP investigation of subcritical instabilities of a cylinder in crossflow. *Exp Fluids*, 56 (10):1–14, 2015.

R.E. Falco and C.P. Gendrich. *Near-Wall Turbulence*, chapter The turbulence burst detection algorithm of Z. Zaric, page 911.931. 1990.

U. Fey and Y. Egami. *Springer Handbook of Experimental Fluid Mechanics*, chapter Transition-Detection by Temperature-Sensitive Paint, pages 537–552. Springer-Verlag, Berlin, Heidelberg, New York, 2007.

U. Fey, Y. Egami, and C. Klein. Temperature-sensitive paint application in cryogenic wind tunnels: Transition detection at high Reynolds numbers and influence of the technique on measured aerodynamic coefficients. In *22nd International Congress on Instrumentation in Aerospace Simulation Facilities, Pacific Grove, CA, 2007*, 2007.

U. Fey, C. Klein, T.J. Möller, J. Pöttner, R. Radespiel, V. Ondrus, and U. Beifuß. *Notes on Numerical Fluid Mechanics and Multidisziplinary Design*, volume 121, chapter Investigation of Circular Cylinder Flow in Water Using Temperature-Sensitive Paint, pages 657–664. Springer-Verlag, 2013.

S. Ghiaasiaan. *Convective Heat and Mass Transfer*. Cambridge University Press, 2011.

H. Guo, V.I. Borodulin, Y.S. Kachanov, C. Pan, J.J. Wang, Q.X. Lian, and S.F. Wang. Nature of sweep and ejection events in transitional and turbulent boundary layers. *Journal of Turbulence*, 11(34):1–51, 2010.

F.R. Hama and J. Nutant. Detailed flow-field observations in the transition process in a thick boundary layer. In *Proceedings of the 1963 Heat Transfer and Fluid Mechanics Institute, Stanford University Press*, 1963.

Y.S. Kachanov. On resonant breakdown of laminar boundary layer. In *Proc. Fifth Natl. Congr. on Theoret. & Appl. Mech., Actual and Topical Problems of Ship Hydro- and Aerodynamics, 1985. 3: 71-1–71-11. Varna: Bulg. Ship Hydrodyn. Cent. (In Russian)*, 1985.

Y.S. Kachanov. Physical mechanisms of laminar-boundary-layer transition. *Annu. Rev. Fluid Mech.*, 26:411–482, 1994.

Y.S. Kachanov and V.Y. Levchenko. The resonant interaction of disturbances at laminar-turbulent transition in a boundary layer. *J. Fluid Mech.*, 138:209–247, 1984.

P. S. Klebanoff, K. D. Tidstrom, and L. M. Sargent. The three-dimensional nature of boundary-layer instability. *J. Fluid Mech.*, 12(1):1–34, 1962.

C. Klein, R.H. Engler, U. Henne, and W.E. Sachs. Application of pressure-sensitive paint for determination of the pressure field and calculation of the forces and moments of models in a wind tunnel. *Exp Fluids*, 39:475–483, 2005. doi: doi:10.1007/s00348-005-1010-8.

D. Kruse. Implementierung eines Störgenerators für kontrollierte Transition mit anschlieÃ§ender Untersuchung der erzeugten Störung. Bachelor's thesis, Institut für Aerodynamik und Gasdynamik, Universität Stuttgart, 2016.

M. Kruse. *Einsatz der Laser-Doppler-Anemometrie zur Untersuchung des laminar-turbulenten Grenzschichtumschlags an der ebenen Platte*. PhD thesis, Universität Stuttgart, 1997.

M. Kruse and S. Wagner. Visualization and laser Doppler measurements of the development of Lambda vortices in laminar-turbulent transition. *Meas. Sci. Technol.*, 9(4): 659–669, 1998.

J. Lemarechal, M. Costantini, C. Klein, M.J. Kloker, W. Wuerz, H.B.E. Kurz, and S. Schaber. Investigation of stationary-crossflow-instability induced transition with temperature-sensitive paint method. In *5th International Conference on Experimental Fluid Mechanics âĂŞ ICEFM 2018 Munich, Munich, Germany, July 2-4, 2018*, 2018a.

J. Lemarechal, C. Klein, U. Henne, D.K. Puckert, and U. Rist. Transition delay by oblique roughness elements in a Blasius boundary-layer flow. In *2018 AIAA Aerospace Sciences Meeting, AIAA SciTech Forum*, number AIAA 2018-1057, 2018b.

J. Lemarechal, C. Klein, U. Henne, D.K. Puckert, and U. Rist. Spatially and temporally resolved visualization of turbulents spots in Blasius boundary layer transition. In *18th International Symposium on Flow Visualization ISFV 18, June 26-29, 2018, Zurich, Switzerland*, 2018c. doi: 10.3929/ethz-b-000279144.

H.-T. Lin. The analogy between fluid friction and heat transfer of laminar forced convection on a flat plate. *Wärme- und Stoffübertragung*, 29:181–184, 1994.

T. Liu and J. P. Sullivan. *Pressure And Temperature Sensitive Paints*. Springer-Verlag, 2005.

R. Narasimha. The laminar-turbulent transition zone in the boundary layer. *Prog. Aerospace Sci.*, 22:29–80, 1985.

V. Ondrus, R. J. Meier, C. Klein, U. Henne, M. Schäferling, and U. Beifuß. Europium 1,3-di(thienyl)propane-1,3-diones with outstanding properties for temperature sensing. *Sensors and Actuators, A: Physical*, 233:434–441, 2015.

F.K. Owen. Transition experiments on a flat plate at subsonic and supersonic speeds. *AIAA Journal*, 8(3):518–523, 1970.

M. Pastuhoff, D. Yorita, K. Asai, and P.H. Alfredsson. Enhancing the signal-to-moise ratio of pressure sensitive paint data by singular value decomposition. *Meas. Sci. Technol.*, 24(7):075301, 2013. doi: doi:10.1088/0957-0233/24/7/075301.

R. Petzold and R. Radespiel. Transition on a wing with spanwise varying crossflow and linear stability analysis. *AIAA Journal*, 53(2):321–335, 2015.

Dominik K Puckert and Ulrich Rist. Experiments on critical reynolds number and global instability in roughness-induced laminar–turbulent transition. *Journal of Fluid Mechanics*, 844:878–904, 2018.

M. Raffel, C.B. Merz, T. Schwermer, and K. Richter. Differential infrared thermography for boundary layer transition detection on pitching rotor blade models. *Exp Fluids*, 56(2):1–22, 2015.

U. Rist. *Numerische Untersuchung der räumlichen, dreidimensionalen Störungsentwicklung beim Grenzschichtumschlag*. PhD thesis, Inst. A f. Mech. Univ. Stuttgart, 1990.

U. Rist and H. Fasel. Direct numerical simulation of control transition in a flat-plate boundary layer. *J Fluid Mech*, 298: 211–248, 1995.

I. Rudolph. *Infrared Thermography as a Tool for Wall Shear Stress Measurements*. PhD thesis, Technische Universität Berlin, 2011.

D. R. Sabatino and C. R. Smith. Turbulent spot flow topology and mechanisms for surface heat transfer. *Journal of Fluid Mechanics*, 612:81–105, 2008.

G.B. Schubauer and H.K. Skramstad. Laminar-boundary-layer oscillations and transition on a flat plate. Technical report, NACA Report No. 909, 1948.

M. Strunz and J.F. Speth. A new laminar water tunnel to study the transition process in a Blasius boundary layer and in a separation bubble and a new tool for industrial aerodynamics and hydrodynamic research. *AGARD CP-413*, pages 25–1–25–5, 1987.

A Subasi, D. Puckert, H. Gunes, and U. Rist. Calibration of constant temperature anemometry with hot-film probes for low speed laminar water channel flows. In *13th International Symposium on Fluid Control, Measurement and Visualization FLUCOME2015, 15-18 November Doha, Qatar*, 2015.

Y.X. Wang and M. Gaster. Effect of surface steps on boundary layer transition. *Exp Fluids*, 39:679–686, 2005.

A. Weiss, A.D. Gardner, C. Klein, and M. Raffel. Boundary-layer transition measurements on mach-scalled helicopter rotor bblade in climb. *CEAS Aeronaut J*, 8:613–623, 2017.

F.M. White. *Viscous Fluid Flow*. Third Edition, McGraw-Hill, New York, International Edition, 2006.

T. Wiegand, H. Bestek, S. Wagner, and H. Fasel. Experiments on a wave train emanating from a point source in a laminar boundary layer. In *26th AIAA Fluid Dynamics Conference, 19-22 June 1995, San Diego, CA*, number AIAA-95-2255, 1995.

D. Yorita, Lemarechal, C. Klein, K. Fujita, and H. Nagai. Dynamic visualization of boundary-layer transition in a pitch-sweep test using a carbon nanotube TSP. In *18th International Symposium on Flow Visualization ISFV 18, June 26-29, 2018, Zurich, Switzerland*, 2018.